Jurnal Presipitasi
Media Komunikasi dan Pengembangan Teknik Lingkungan
e-ISSN: 2550-0023

Vol 23, No 1, 2026, 244-257
Article available at homepage presipitasi

Regional Case Study

Interannual Climate Variability Impacts on Rainfall Extremes and Flooding

Jogi Panggabean[1*], Fadli Syamsudin[1,2], Suaydhi[2], Noir Purba[1], Xingru Feng[3]

[1] Marine Science Program, Faculty of Fisheries and Marine Sciences, Universitas Padjadjaran, Jalan Raya Bandung – Sumedang KM 21, Jatinangor, Indonesia 45363

[2] Research Center for Climate and Atmosphere, Badan Riset dan Inovasi Nasional, Jalan Dr. Djunjunan No. 133, Jakarta, Indonesia 133. Bandung, Indonesia 40135

[3] Key Laboratory of Ocean Observation and Forecasting & Laboratory of Ocean Circulation and Waves, Institute of Oceanology Chinese Academy of Sciences, 7 Nanhai Rd, Shinan Disctrict, Qingdao, China 266071

* Corresponding Author, email: jogi22001@mail.unpad.ac.id

Abstract

The Bandung metropolitan region has faced escalating flood threats (2014–2024); however, oceanic climate–rainfall relationships remain uninvestigated. This study investigates the interannual climate variability influencing extreme precipitation and flooding using historical records and the GPM-IMERG satellite measurements, which had a 90.4% correlation with BMKG. Bojongsoang (117 events), Lembang (49 events), and Braga (42 events) emerge as highest-risk areas. The peak flooding in January 2020 (15 events) coincided with the La Niña and negative Indian Ocean Dipole (IOD) phases. The average daily maximum rainfall during the wet season was 62 mm, compared with 41 mm in the dry season, with 36 heavy rain days versus 8 days. La Niña increased heavy rain days to 62.5 days compared with El Niño (38.6 days) and extreme rainfall to 399.6 mm versus 244.2 mm. Negative IOD enhanced the daily maximum to 76.8 mm versus 56.8 mm during the positive phases. Flood months showed 81.3 heavy rain days versus 14.4 in normal months. Early warning thresholds were established at >70 mm daily maximum, >60 heavy rain days, and >400 mm extreme precipitation.

Keywords: Climate variability; el niño-southern oscillation; extreme precipitation; floods; indian ocean dipole; madden-julian oscillation

1. Introduction

Year-to-year oceanic climate fluctuations have surfaced as primary drivers of precipitation pattern modifications worldwide, with progressively severe influences on extreme meteorological phenomena and flooding risks in tropical areas. The El Niño-Southern Oscillation, Indian Ocean Dipole, and Madden-Julian Oscillation constitute three principal interannual climate variations that govern regional rainfall distribution and magnitude through intricate atmospheric teleconnections. Recent studies have demonstrated that these oscillations can increase extreme precipitation by 40 %–80% above normal conditions when operating in reinforcing phases (Freund et al., 2019).

The current understanding of climate–precipitation relationships has advanced significantly through improved satellite observations and modeling capabilities. Recent research has established

robust teleconnection mechanisms between Indo-Pacific climate modes and regional precipitation extremes across Southeast Asia (Xiao et al., 2022). High-resolution satellite precipitation products now enable detailed analysis of extreme precipitation patterns, whereas advanced statistical methods allow quantification of climate impacts on flood hazards. These technological advances have revealed complex interactions between large-scale climate forcing and local topographic controls in determining flood vulnerability patterns. Despite the growing recognition of interannual climate teleconnection impacts on Indonesian precipitation patterns, significant research gaps remain in understanding these relationships at the metropolitan scale. Few studies have comprehensively quantified climate–precipitation relationships using high-resolution satellite data validated against observed flood occurrences in tropical highland urban environments. This gap is particularly critical in the Greater Bandung region, where unique topographic characteristics create complex precipitation enhancement patterns that interact with climate variability to determine flood hazards. The lack of integrated climate–flood analysis limits the development of climate-informed early warning systems for vulnerable tropical urban areas (Byaruhanga et al., 2024).

This study represents the first comprehensive analysis linking large-scale climate patterns with local flood occurrences in the Greater Bandung tropical highland urban environment. The research aims to quantify the relationships between interannual ocean climate variability and extreme precipitation patterns, evaluate extreme rainfall characteristics through climate indices, and provide insights for developing climate-informed flood hazard management strategies. The novelty lies in integrating satellite–ground data validation with operational threshold development for a topographically complex urban basin that is highly sensitive to climate variability.

2. Methods

The study area encompasses the Greater Bandung metropolitan region in West Java Province, Indonesia, which is positioned at 6°50′-7°50′ S and 107°25′-108°00′ E (Figure 1). The region represents a unique closed basin surrounded by the volcanic mountains Mount Tangkuban Perahu (2,084 m), Mount Manglayang (1,818 m), and Mount Patuha (2,434 m), creating optimal conditions for orographic precipitation enhancement. This topographic configuration renders the area particularly sensitive to interannual climate variability effects on extreme precipitation patterns in tropical urban environments (Kurniadi et al., 2021).

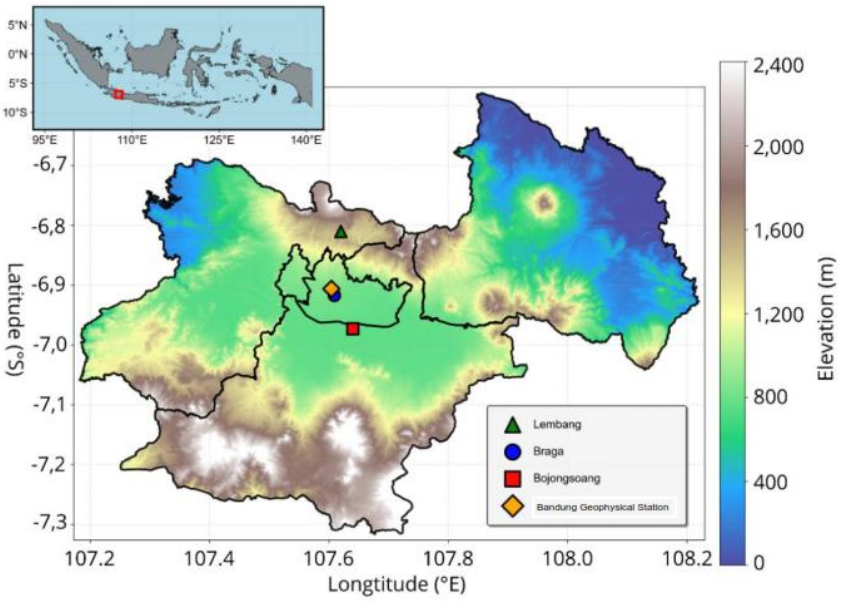

Figure 1. Map of the study area showing the Bandung Basin and surrounding topographic features in West Java, Indonesia. The map displays elevation gradients with the three major volcanic peaks (Mount

Tangkuban Perahu: 2,084 m, Mount Manglayang: 1,818 m, Mount Patuha: 2,434 m) that create a closed basin configuration.

2.1. Tabulation of Hazard Event

Comprehensive flood occurrence data (2014–2024) were compiled from the National Disaster Management Agency Disaster Portal (BNPB) database and cross-validated using regional disaster management records, meteorological stations, and major news sources following established multi-source validation protocols. Spatial clustering analysis employed density-based clustering algorithms using Python's scikit-learn library, implementing DBSCAN clustering with a 5 km radius threshold, to identify flood hotspots and vulnerability patterns across the metropolitan area (Wati et al., 2022). Three primary high-frequency flooding hazard zones were detected through a statistical examination of occurrence density and spatial clustering patterns based on established urban flood susceptibility evaluation methodologies: Bojongsoang (117 flood events), Lembang (49 flood events), and Braga (42 flood events) during the 2014–2024 analysis period. Additional flood occurrence data were integrated from local disaster management agencies, meteorological stations, and regional government reports to ensure comprehensive coverage of flood hazard events (Rentschler et al., 2022).

2.2. Calculation of Precipication Extreme Indices

Extreme precipitation indices were calculated following the updated Expert Team on Climate Change Detection and Indices protocols using best practices for tropical climate analysis (Kim et al., 2020).

Statistical analyses were conducted using R software (version 4.3.0) with the climatology package (version 4.2.0) for quality control and homogenization, the extremes package for extreme value analysis, and the trend package for trend detection.

The maximum 1-day precipitation index (RX1day) was calculated as the annual maximum value of the daily precipitation totals for each grid point across the study area, following established extreme precipitation methodologies. This index directly captures the intensity aspect of precipitation extremes most related to flash flood hazard generation:

$$RX1day = \max(PRCPi) \quad for\ i = 1\ to\ 365\ days \tag{1}$$

where PRCPi represents the daily precipitation on day i. The R10mm index represents the annual number of days with precipitation ≥10 mm, providing a frequency-based measure of moderate-to-heavy precipitation events contributing to cumulative flood hazard.

$$R10mm = \Sigma(PRCPi \geq 10mm) \quad for\ i = 1\ to\ 365\ days \tag{2}$$

The R95p index calculates the total annual precipitation from days exceeding the 95th percentile of wet day precipitation (days ≥1 mm), representing extreme precipitation contributions to seasonal flood hazard:

$$R95p = \Sigma(PRCPi > 95th\ (percentile\ of\ wet\ days)) \tag{3}$$

These indices provide a comprehensive characterization of precipitation intensity, frequency, and extremes, which are relevant to flood hazard assessment in Southeast Asian tropical environments.

2.3. Ocean Climate Indices

Oceanic Niño Index data were obtained from the National Oceanic and Atmospheric Administration Climate Prediction Center, representing the three-month running mean of sea surface temperature anomalies in the Niño 3.4 region (5°N–5 °S, 120°–170 °W). El Niño–Southern Oscillation

phases were classified using updated Oceanic Niño Index criteria: El Niño (Oceanic Niño Index ≥ +0.5°C) and La Niña (Oceanic Niño Index ≤ -0.5°C) for five consecutive seasons (Chen et al., 2012). The Indian Ocean Dipole phases utilized the Dipole Mode Index following recent Indian Ocean Dipole classification refinements: positive (Dipole Mode Index > +0.4 °C) and negative (Dipole Mode Index <-0.4 °C) Indian Ocean Dipoles with an updated understanding of Indian Ocean Dipole impacts on Indonesian precipitation. The Madden–Julian Oscillation employed real-time multivariate Madden–Julian Oscillation indices with recent algorithmic improvements for tropical applications, with active phases defined with an amplitude greater than 1.0 (Cheng et al., 2024).

2.4. Satellite Precipitation Data and Validation

The high-resolution rainfall data employed NASA's Global Precipitation Measurement Integrated Multi-satellite Retrievals Final Run Version 07 (0.1° × 0.1° daily resolution), which depicts the newest generation of satellite rainfall products with improved precision for tropical zones. Rainfall estimates were verified against BMKG ground measurements at Stasiun Geofisika Bandung using comprehensive statistical indicators, including the Pearson correlation coefficient (r), coefficient of determination (R^2), and root mean square error. Advanced bias correction algorithms employed random forest regression implemented in Python using the scikit-learn library with cross-validation to enhance satellite accuracy for extreme precipitation detection (Huffman et al., 2020).

The validation demonstrates exceptional agreement with a Pearson correlation of 0.904 and R^2 of 0.817, explaining 81.7% of precipitation variance across 3,481 data points (Figure 2). Temporal validation shows an accurate capture of both the timing and magnitude of precipitation events throughout 2014–and 2024 successfully identifies extreme events exceeding 100 mm/day, which are critical for flood analysis.

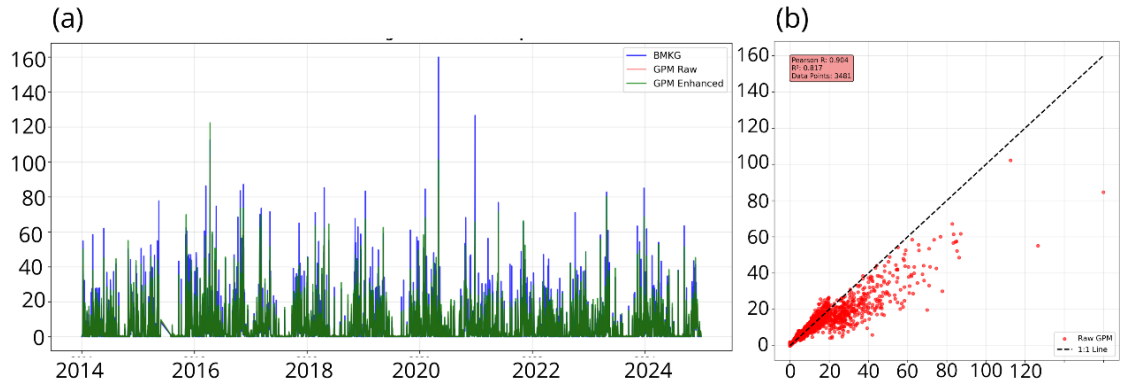

Figure 2. GPM-BMKG satellite precipitation validation at Stasiun Geofisika Bandung (2014-2024). (a) Scatter plot showing strong agreement between GPM and BMKG observations (R^2 = 0.817, r = 0.904, n = 3,481). Dashed line represents 1:1 perfect agreement. (b) Time series comparison of BMKG (blue), GPM raw (red), and GPM enhanced (green) estimates demonstrating temporal accuracy and improvement through bias correction

2.5. Statistical Analysis

Trend analysis applied robust nonparametric methods, including the Mann–Kendall test, with recent modifications for climate trend detection and Sen's slope estimator for magnitude quantification (Henemuth et al., 2013). Spatial analysis utilized advanced Python-based frameworks, including xarray (version 2023.6.0) for multidimensional data processing, Matplotlib (version 3.7.0) with Viridis color palettes for visualization, and Scikit-learn (version 1.3.0) for machine learning applications in teleconnection analysis. High-resolution SRTM digital elevation data were processed using GDAL (version 3.7.0) to quantify orographic enhancement effects.

3. Result and Discussion

3.1. Spatial Distribution of Flood Hazard Events Around Bandung

The spatial clustering analysis reveals pronounced heterogeneity in flood hazard distribution across the Greater Bandung region, with distinct high-risk zones emerging from the density-based clustering methodology. This spatial heterogeneity demonstrates how complex topographic controls interact with urbanization patterns to create differential flood risk exposure in tropical highland urban basins.

Bojongsoang emerges as the area with highest flood frequency (117 events), located in the southern-central basin where multiple highland drainage channels converge into the central depression. This exceptional vulnerability reflects the basin's natural drainage convergence patterns, in which the topographic configuration creates optimal conditions for flood accumulation during extreme precipitation events. Lembang shows the second highest flood frequency (49 events), positioned in the northern portion near Mount Tangkuban Perahu slopes. This pattern reflects the complex interaction between orographic precipitation enhancement and urban drainage limitations in the transition zone between highland and lowland areas. Braga had the third highest flood frequency (42 events), demonstrating how local topographic and drainage characteristics create systematic vulnerability patterns within the metropolitan region.

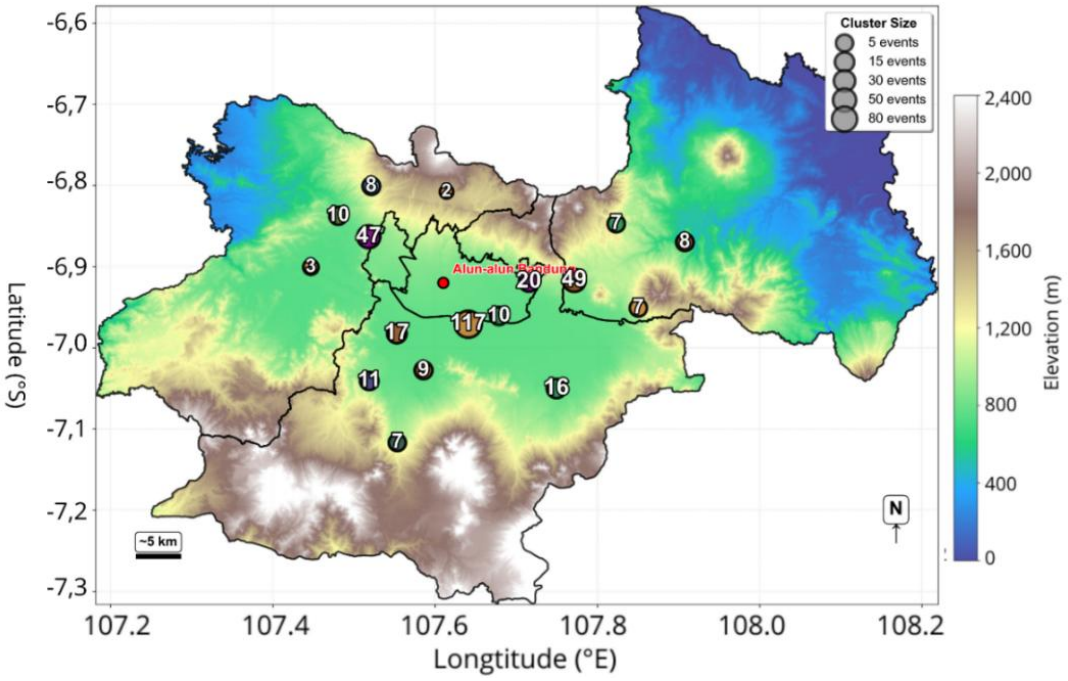

Figure 3. Spatial distribution map of flood hazard events across the Greater Bandung region during 2014–2024. The map displays topographic features with elevation gradients (0–2, 400 m) and flood event clusters using proportional symbols (5–80 events). The major flood-prone areas are Bojong Soang (117 events), Lembang (49 events), and Braga (42 events). A closed basin configuration surrounded by volcanic peaks creates distinct vulnerability zones, with the highest frequencies occurring in low-lying convergence areas. Elevation data were derived from the SRTM digital elevation model.

3.2. Time Series of Flood Events

A temporal analysis of flood hazard events revealed pronounced interannual and seasonal variability, with distinct epochal behavior reflecting the strong influence of large-scale climate forcing on regional flood occurrence patterns (Figure 4). This temporal structure demonstrates the critical role of interannual climate variability in modulating flood hazards through systematic changes in atmospheric circulation patterns that influence regional precipitation characteristics. The temporal patterns show clear

correspondence with major climate oscillation phases, indicating strong teleconnection mechanisms between Indo-Pacific climate modes and regional flood hazard occurrence. The monthly flood event time series demonstrates significant modulation by interannual climate variability, reflecting the sensitivity of tropical precipitation systems to large-scale atmospheric circulation anomalies associated with the El Niño-Southern Oscillation, Indian Ocean Dipole, and Madden-Julian Oscillation (Sheng et al., 2023).

January 2020 recorded the most exceptional flood hazard period, with 15 flood events in a single month, which is unprecedented during the study period. This extraordinary concentration occurred because of the simultaneous occurrence of strong La Niña conditions and negative Indian Ocean Dipole phases, creating compound effects of multiple climate modes in reinforcing phases. The temporal analysis reveals that this extreme period demonstrates how favorable climate conditions can align to create compound extreme events with exceptional impact potential. Such extreme flood activity periods reflect optimal atmospheric conditions for sustained extreme precipitation generation, consistent with observations of compound climate impacts on Indonesian precipitation extremes documented in recent studies (Panggabean et al., 2025).

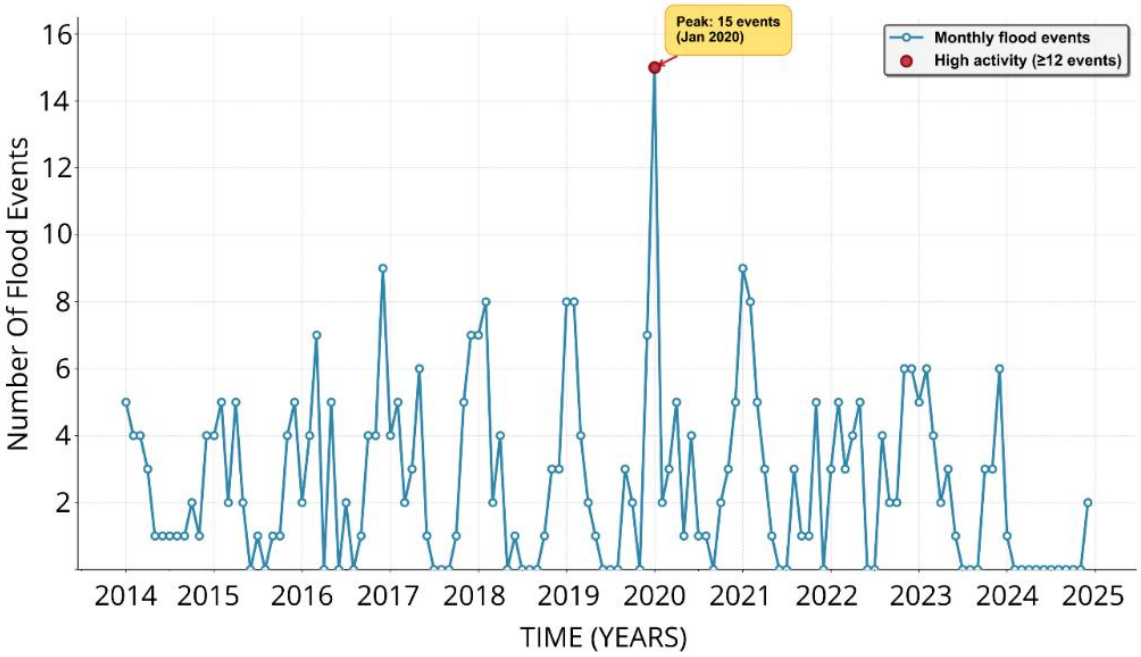

Figure 4. Monthly flood event time series for the Greater Bandung region (2014–2024) showing temporal variability and peak flood activity periods. The time series reveals distinct epochal behavior with alternating active and quiescent phases. Notable features include a peak in activity in January 2020 (15 events) and high activity periods (≥12 events), marked in red.

3.3. Maximum 1-Day Precipitation (RX1day)

The RX1day index demonstrates systematic seasonal variability with consistent basin-wide enhancement during wet periods and systematic orographic controls throughout the annual cycle (Figure 5). This seasonal pattern demonstrates how the Indonesian monsoon system exerts fundamental control over extreme precipitation distribution through systematic changes in atmospheric circulation patterns, moisture transport efficiency, and convective activity across the region. The analysis reveals systematic seasonal variability that reflects the strong influence of the Indonesian monsoon system on extreme precipitation distribution, consistent with established monsoon precipitation climatology across Southeast Asia, as documented in comprehensive recent studies (Jiang et al., 2022).. These seasonal patterns align with findings from Jakarta, where similar monsoon-driven precipitation extremes have been documented, suggesting regional consistency in climate–precipitation relationships across West Java.

The wet season from December to February records the highest daily precipitation extremes, with a basin mean of 62 mm and maximum intensities reaching 89 mm in mountainous regions. Spatial distribution analysis reveals that these maximum values occur consistently along windward mountain slopes, where forced orographic lifting enhances precipitation intensity by 30 %–50% compared to lowland areas. The March to May transition period maintains comparable intensity levels (mean: 65 mm, maximum: 76 mm) with a more spatially uniform distribution, reflecting the transitional nature of monsoon circulation patterns. The June to August dry season shows a substantial reduction (mean: 41 mm, maximum: 60 mm) due to weakened monsoon circulation, whereas the September to November period demonstrates recovery patterns (mean 65 mm, max: 90 mm) as monsoon circulation begins to strengthen (Nur'utami and Hidayat, 2016).

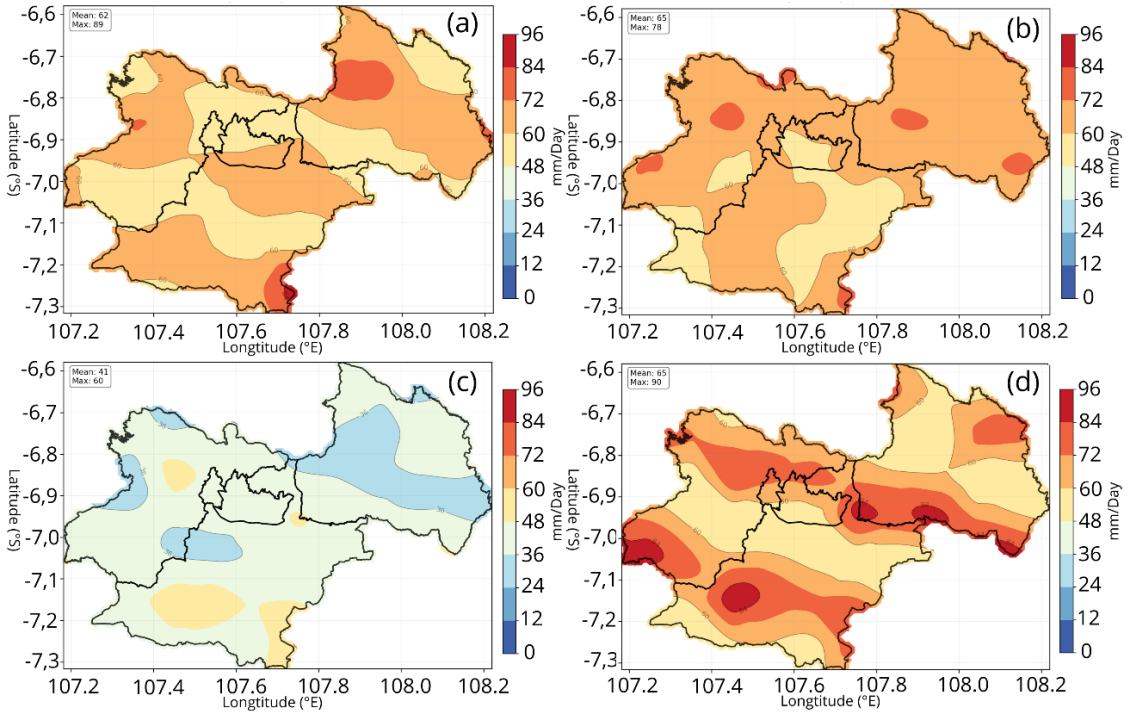

Figure 5. Seasonal spatial distribution of RX1day (maximum 1-day precipitation) across the Greater Bandung region for 2014-2024. (a) DJF (mean: 62 mm, max: 89 mm), (b) MAM (mean: 65 mm, max: 76 mm), (c) JJA (mean: 41 mm, max: 60 mm), and (d) SON (mean: 65 mm, max: 90 mm)

3.4. Heavy Precipitation Days (R10mm)

The R10mm index reveals dramatic seasonal contrasts, reflecting the distinct wet-dry seasonality characteristic of the Indonesian monsoon system (Figure 6). The seasonal contrast occurs because fundamental changes in atmospheric circulation patterns associated with monsoon transitions create sustained atmospheric moisture availability during the wet season, while causing severe precipitation suppression during the dry season due to large-scale circulation changes. This pronounced seasonality aligns with established monsoon precipitation patterns across the Indonesian Maritime Continent, where wet-season precipitation frequency can exceed dry-season values by factors of 3–5.

The December to February wet season is characterized by frequent heavy precipitation (basin mean: 36 days; maximum frequency: 41 days) in the northern highland areas. This high frequency occurs because sustained atmospheric moisture availability throughout the primary wet season period supports consistent precipitation activity when monsoon circulation patterns favor moisture transport and convective activity. The March to May transition period shows moderate activity (mean: 30 days; maximum frequency: 33 days), reflecting the gradual strengthening of monsoon circulation. The June to August dry season shows extreme suppression (mean: 8 days; maximum frequency: 10 days) because the

dominant influence of dry continental air masses during the southeast monsoon period creates large-scale circulation patterns that favor subsidence and moisture divergence. The September to November transition demonstrates gradual recovery (mean: 21 days; maximum frequency: 25 days) as monsoon circulation begins to strengthen, reflecting the transitional nature of pre-monsoon atmospheric conditions.

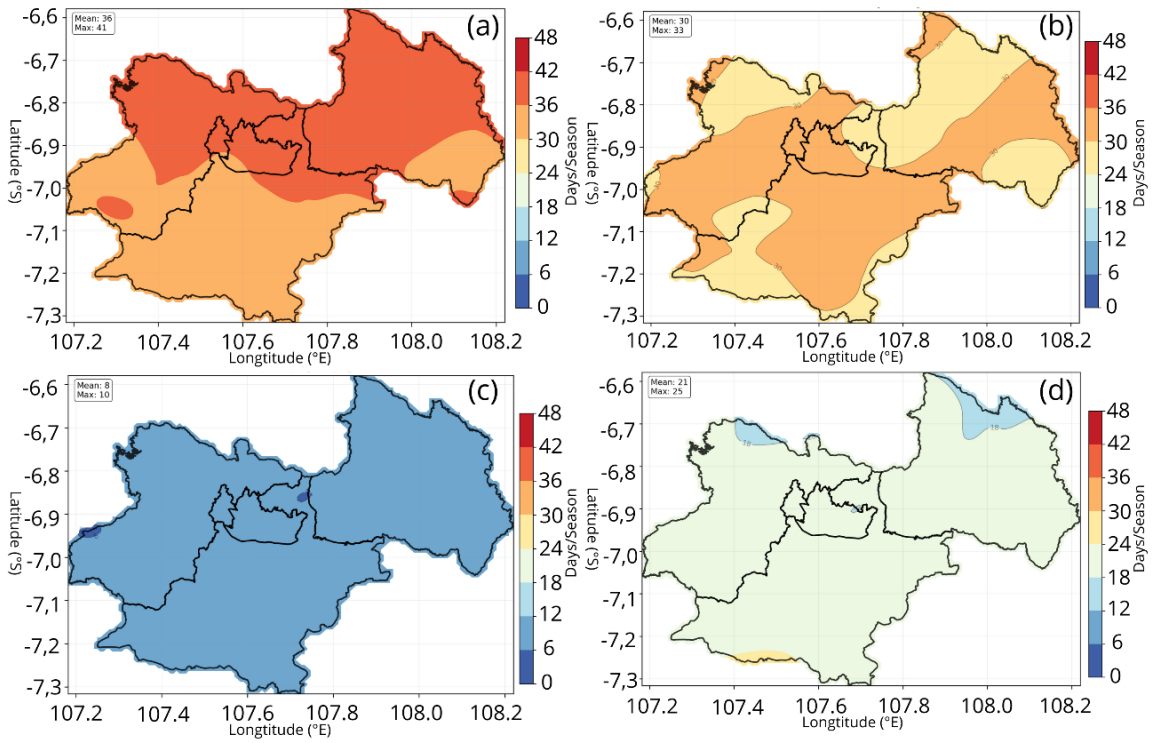

Figure 6. Seasonal spatial distribution of R10mm (heavy precipitation days) across the Greater Bandung region from 2014 to 2024. Four panels illustrate: (a) DJF peak frequency (mean: 36 days, max: 41 days), (b) MAM moderate activity (mean: 30 days, max: 33 days), (c) JJA minimum activity (mean: 8 days, max: 10 days), and (d) SON recovery period (mean: 21 days, max: 25 days).

3.5. Very Wet Day Precipitation (R95p)

The R95p index exhibited the most pronounced seasonal variability among all extreme precipitation metrics, with values ranging from 64 to 386 mm across different seasons and locations (Figure 7). This extreme seasonal range demonstrates how monsoon circulation strength and moisture availability fundamentally control the characteristics of precipitation extremes, with wet-season conditions supporting sustained extreme precipitation events and dry-season conditions severely limiting extreme precipitation potential. The seasonal range occurs because the strong sensitivity of precipitation extremes to monsoon circulation strength creates optimal conditions for sustained extreme precipitation generation during the wet season while severely limiting extreme precipitation potential during the dry season. This extreme seasonal range reflects the strong sensitivity of precipitation extremes to monsoon circulation strength and moisture availability, consistent with documented extreme precipitation variability across tropical Southeast Asia.

The December to February period exhibits maximum extreme precipitation intensity, characterized by basin-wide mean values of 264 mm and peak intensities reaching 386 mm in orographically enhanced regions. Spatial analysis reveals distinct enhancement patterns, including persistent extreme precipitation hotspots on the northern slopes of Mount Tangkuban Perahu and the southeastern highlands. These spatial patterns arise from the optimal orientation for orographic lifting of moisture-laden air masses from the Java Sea, generating systematic precipitation enhancement zones that

represent persistent extreme precipitation and flood hazard areas. The basin's closed topographic configuration establishes systematic precipitation gradients, resulting in differential flood hazard exposure across the region, with mountainous areas receiving substantially higher extreme precipitation totals than lowland areas, despite concentrated flood occurrences in convergence zones.

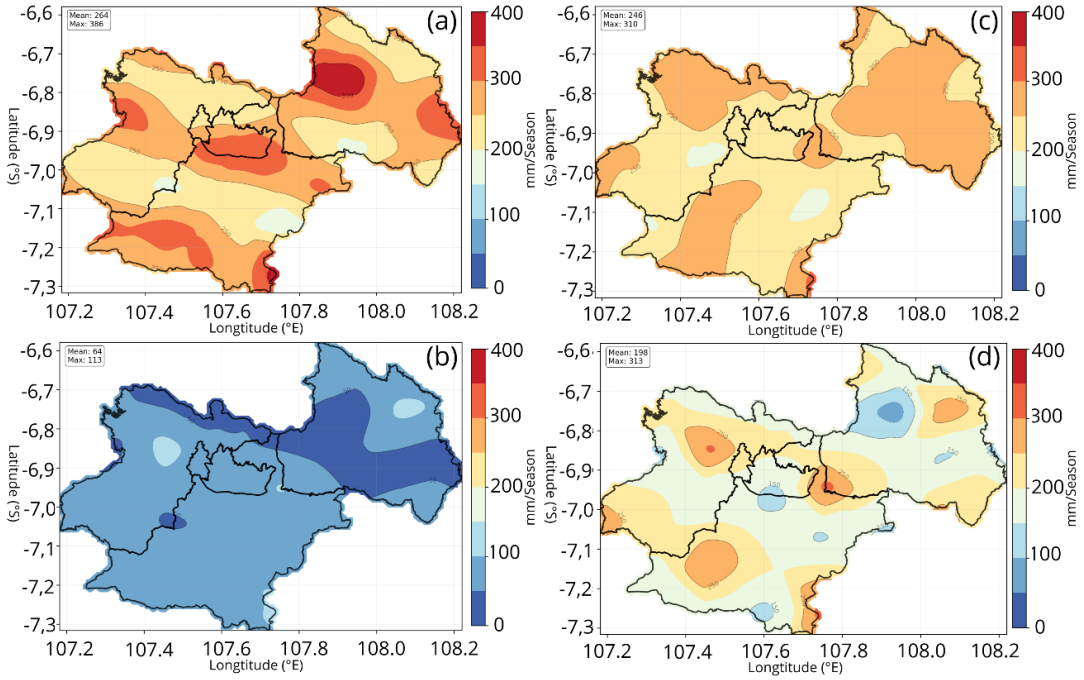

Figure 7. Seasonal spatial distribution of R95p (very wet day precipitation) across the Greater Bandung region for 2014–2024. Four panels show (a) DJF wet season with maximum values (mean: 264 mm, max: 386 mm), (b) MAM transition period (mean: 246 mm, max: 310 mm), (c) JJA dry season with minimum values (mean: 64 mm, max: 113 mm), and (d) SON transition period (mean: 198 mm, max: 313 mm).

3.6. ENSO Influence on Rainfall Extremes and Flood Hazard

El Niño-Southern Oscillation (ENSO) phases demonstrate systematic and statistically significant impacts on extreme precipitation across the Greater Bandung region, with La Niña conditions consistently enhancing precipitation, whereas El Niño phases suppress extremes (Figure 8). These results demonstrate how large-scale ocean–atmosphere coupling fundamentally modulates regional precipitation extremes through systematic changes in atmospheric circulation patterns, moisture transport efficiency, and convective activity. The influence of the ENSO operates through well-established teleconnection mechanisms that systematically alter atmospheric circulation patterns, moisture availability, and convective activity across the Indonesian Maritime Continent. These results align with established ENSO teleconnection patterns affecting Indonesian precipitation, in which La Niña typically enhances wet-season precipitation through strengthened monsoon circulation and increased moisture transport.

Heavy precipitation frequency (R10 mm) shows the strongest El Niño-Southern Oscillation (ENSO) response, with La Niña generating 62.5 days annually, compared with 38.6 days during El Niño (61.9% increase, $p < 0.001$). This substantial increase occurs because La Niña conditions systematically strengthen monsoon circulation patterns and enhance moisture transport efficiency, creating optimal conditions for sustained heavy precipitation events throughout the wet season. Very wet day precipitation (R95p) exhibits substantial enhancement during La Niña (399.6 mm vs. 244.2 mm in El Niño, 63.6% increase), reflecting the strong sensitivity of extreme precipitation to ENSO-related atmospheric circulation anomalies that systematically alter moisture transport and convective activity patterns across the region. The spatial coherence of ENSO impacts across the basin, with peak anomalies concentrated

along orographically favored mountain slopes, demonstrates the interaction between large-scale climate forcing and local topographic controls.

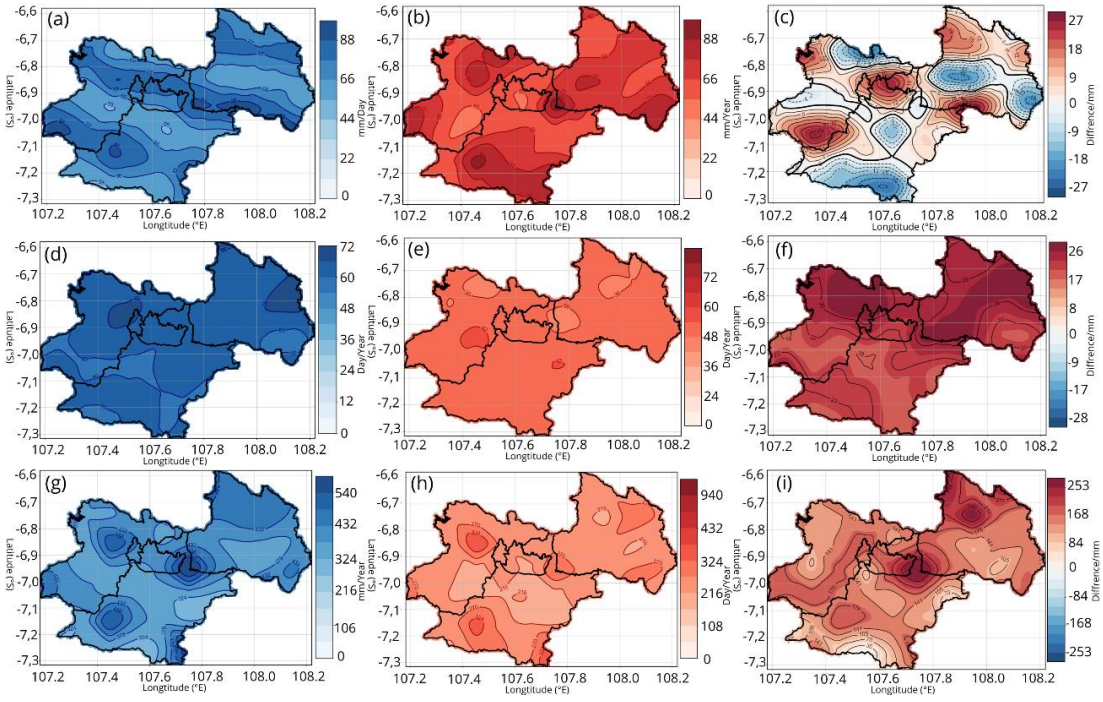

Figure 8. Extreme precipitation patterns during La Niña vs. El Niño phases (2014–2024). Panels show (a,d, and g) La Niña conditions, (b,e, and h) El Niño conditions, and (c,f, and i) differences (La Niña minus El Niño). Top row: RX1day maximum daily precipitation. Middle row: R10mm heavy precipitation days. Bottom row: R95p seasonal extreme precipitation.

3.7. Indian Ocean Dipole Role in Regional Flood Hazard

The Indian Ocean Dipole shows a particularly strong influence on extreme precipitation around Bandung, with notable impacts across multiple precipitation indices (Figure 9). This strong influence demonstrates how Indonesia's strategic position within the Indian Ocean basin maximizes exposure to Indian Ocean Dipole teleconnection effects, with negative Indian Ocean Dipole phases creating optimal conditions for enhanced moisture transport and precipitation intensification across the region. The Indian Ocean Dipole influence operates through systematic changes in Indian Ocean sea surface temperature patterns that fundamentally alter regional atmospheric circulation and moisture transport patterns. This strong influence reflects Indonesia's strategic position within the Indian Ocean basin, where Indian Ocean Dipole teleconnections are maximized, consistent with the established understanding of Indian Ocean Dipole impacts on Indonesian precipitation patterns.

Maximum daily precipitation (RX1day) demonstrated notable sensitivity to the Indian Ocean Dipole (IOD), with negative phases producing 76.8 mm of precipitation, compared with 56.8 mm during positive phases (35.2% enhancement, $p < 0.001$). This enhancement occurred because negative IOD phases created anomalously warm sea surface temperatures west of Sumatra, which strengthened the regional Walker circulation and intensified convective activity across the Indonesian Maritime Continent. High precipitation frequency (R10mm) showed strong IOD modulation (34.0 days vs. 20.3 days, 67.5% increase), whereas R95p exhibited substantial enhancement during negative IOD (278.8 mm vs. 183.2 mm, 52.2% increase). These substantial increases occurred because IOD phases fundamentally altered regional precipitation regimes, with negative IOD events creating conditions favorable for sustained extreme precipitation generation that significantly elevated the flood hazard potential. The timing of IOD impacts coincided optimally with the regional wet season (December–March), when atmospheric moisture

availability peaked, and monsoon circulation facilitated efficient moisture transport from the tropical Indian Ocean toward West Jawa (Ratna et al., 2021).

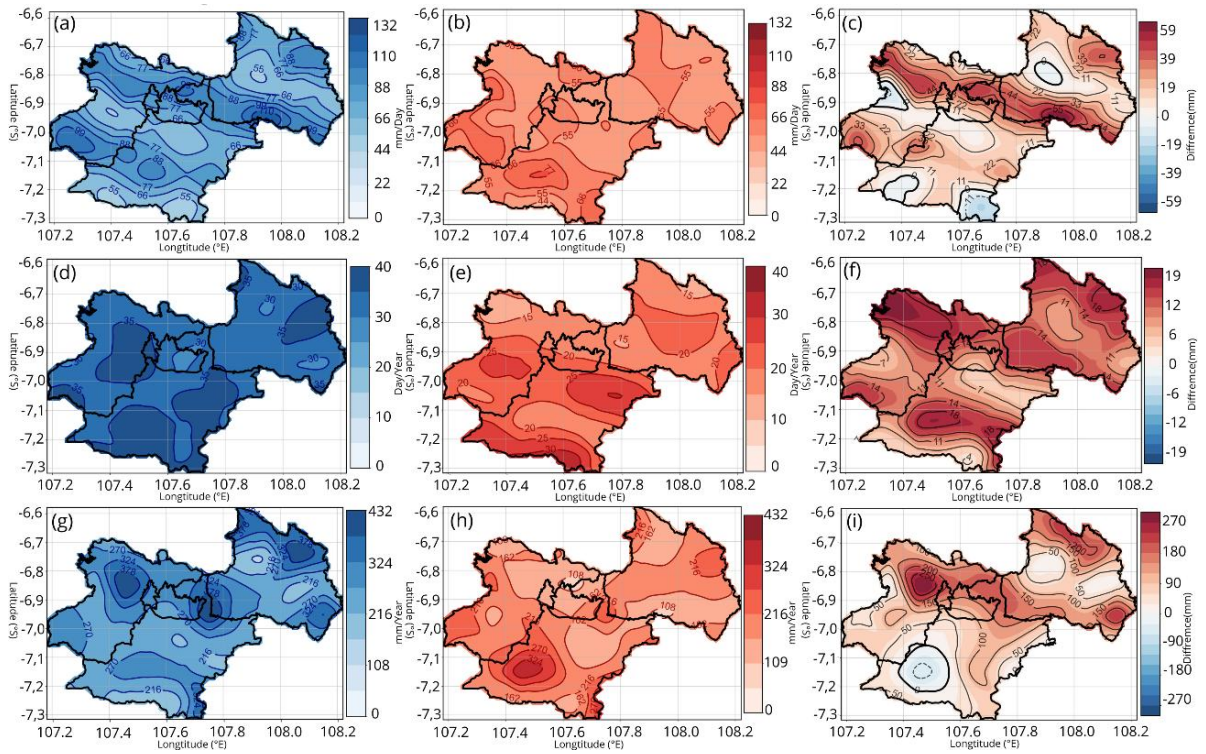

Figure 9. Extreme precipitation patterns during Indian Ocean Dipole phases (2014–2024). Panels show (a,d, and g) negative IOD conditions, (b,e, and h) positive IOD conditions, and (c,f, and i) differences (negative minus positive). Top row: RX1day maximum daily precipitation. Middle row: R10mm heavy precipitation days. Bottom row: R95p seasonal extreme precipitation.

3.8. Flood Hazard Verification

Statistical validation reveals strong relationships between extreme precipitation indices and observed flood occurrences, providing robust support for satellite-based flood hazard assessment (Figure 10). The validation demonstrates clear precipitation threshold effects that distinguish flood from non-flood conditions, supporting the development of quantitative operational early warning criteria based on satellite precipitation monitoring. This validation provides strong empirical evidence for the utility of satellite-derived precipitation metrics in operational flood forecasting applications. High precipitation frequency (R10 mm) demonstrated the strongest discrimination capability, with an average of 81.3 days of flood events compared with 14.4 days during non-flood periods (464% increase, $p < 0.001$). This dramatic difference occurs because flood generation requires sustained heavy precipitation events that accumulate sufficient water volume to exceed drainage system capacity.

Very wet day precipitation (R95p) shows substantial enhancement during floods (524.9 mm vs. 110.3 mm, 376% increase), while maximum daily precipitation (RX1day) averages 80.3 mm during flood events compared with 40.9 mm in non-flood periods (96% increase). These dramatic differences validate the use of satellite-derived precipitation metrics for operational flood forecasting applications, demonstrating that precipitation indices can serve as reliable proxies for flood hazard assessment in tropical urban environments (Budiyono et al., 2015).

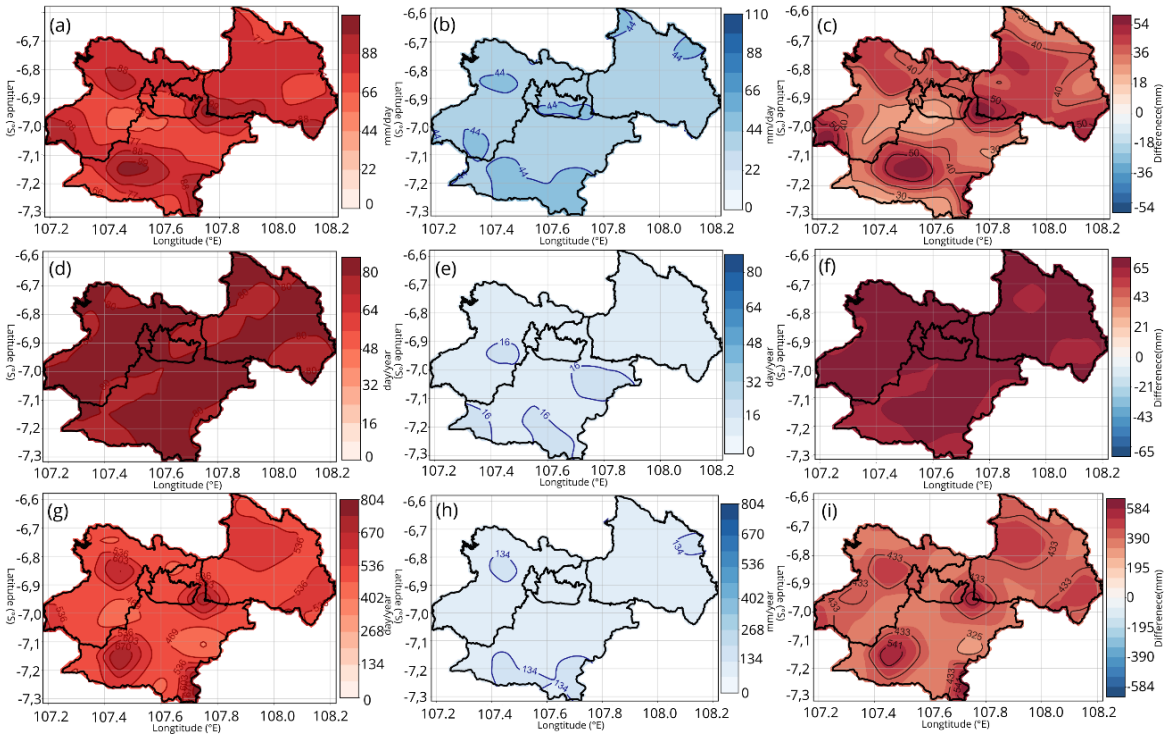

Figure 10. Precipitation comparison between flood and normal conditions (2014–2024). Panels show (a,d, and g) flood event months, (b,e, and h) non-flood months, and (c,f, and i) differences (flood minus non-flood). Top row: RX1day maximum daily precipitation. Middle row: R10mm heavy precipitation days. Bottom row: R95p seasonal extreme precipitation.

4. Conclusions

This study provides evidence for the significant influence of interannual ocean climate variability on extreme precipitation and flood hazards in Bandung, Indonesia. Large-scale climate oscillations modulate regional precipitation extremes through teleconnection. This creates distinct flood vulnerability patterns across the Greater Bandung region. The spatial flood hazard analysis showed pronounced heterogeneity. Bojongsoang had the highest flood frequency (117 events). Lembang follows with 49 events. Braga has 42 events. A closed basin topography creates natural convergence zones. Surface runoff accumulated in these areas. This amplifies flood vulnerability in low-lying areas. Interannual climate variability controls the timing and intensity of flood hazards. The Indian Ocean Dipole shows substantial influence during negative phases. These phases enhance the maximum daily precipitation. The El Niño-Southern Oscillation demonstrates considerable impacts. La Niña conditions increase the frequency of heavy precipitation. Heavy precipitation frequency responded to both climate modes. This shows the importance of sustained precipitation events for flood generation.

Extreme precipitation indices exhibit seasonal variability. This variability is consistent with Indonesian monsoon dynamics. The wet season records higher values across all metrics compared with the dry season. Orographic enhancement produces elevated precipitation on windward mountain slopes. Northern and southeastern highland areas are persistent extreme precipitation zones. Satellite data validation reveals strong relationships between precipitation indices and observed flooding. Operational thresholds have been identified for various precipitation indices. Extreme rainfall greater than 70 mm daily maximum provides an early flood warning criterion. Greater than 60 heavy rain days also provide warning criteria. Greater than 400 mm extreme precipitation provides additional warning criteria. Interannual ocean climate variability operates as an important driver of flood hazard modulation around Bandung. The Indian Ocean Dipole and El Niño-Southern Oscillation effects are combined with local topographic amplification. This creates complex vulnerability patterns. These findings contribute to

understanding of climate-flood relationships. They support development of improved forecasting approaches for disaster risk reduction in tropical urban environments.

Acknowledgement

The authors express sincere gratitude to the Faculty of Fisheries and Marine Sciences, Universitas Padjadjaran; the Research Center for Climate and Atmosphere, National Research and Innovation Agency; and the Key Laboratory of Ocean Observation and Forecasting & Laboratory of Ocean Circulation and Waves, Institute of Oceanology, Chinese Academy of Sciences, Qingdao, China, for institutional support and research facilities. We extend appreciation to BMKG for ground-based precipitation data, NASA for Global Precipitation Measurement Integrated Multi-satellite Retrievals satellite data, NOAA for oceanic climate indices, and BNPB for flood occurrence data.

Ethics Statement

This study was conducted using publicly available secondary data from official sources, including BMKG (Badan Meteorologi, Klimatologi, dan Geofisika) for ground-based precipitation records, NASA for Global Precipitation Measurement Integrated Multi-satellite Retrievals satellite data, NOAA for oceanic climate indices, and BNPB for flood occurrence data. No primary data collection involving human participants or animals was performed. Therefore, ethical approval and informed consent were not required for this research.

CRediT Author Statement

Jogi Panggabean: Idea Development, Research Design, Investigation, Formal Analysis, Data Curation, Visualization, Manuscript Draft Preparation, Manuscript Review and Revision. **Fadli Syamsudin:** Supervision, Research Design, Manuscript Review and Revision. **Suaydhi:** Supervision, Resources, Manuscript Review and Revision. **Noir Purba:** Supervision, Manuscript Review and Revision. **Xingru Feng:** Resources, Supervision, Manuscript Review and Revision.

References

Budiyono, Y., Aerts, J., Brinkman, J, J., Marfai, M, A. and Ward, P. 2015. Flood risk assessment for delta mega-cities: a case study of Jakarta. Natural Hazards 75, 389–413.

Byaruhanga, N., Kibirige, D., Gokool, S., and Mkhonta, G. 2024. Evolution of flood prediction and forecasting models for flood early warning systems: a scoping review. Water (Switzerland) 16, 1–29.

Chen, H., Sun, J., Chen, X., and Zhou, W. 2012. CGCM projections of heavy rainfall events in China. International Journal of Climatology 32, 441–450.

Cheng, L., Abraham, J., Trenberth, K.E., Boyer, T., Mann, M.E., Zhu, J., Wang, F., Yu, F., Locarnini, R., Fasullo, J., Zheng, F., Li, Y., Zhang, B., Wan, L., Chen, X., Wang, D., Feng, L., Song, X., Liu, Y., Reseghetti, F., Simoncelli, S., Gouretski, V., Chen, G., Mishonov, A., Reagan, J., Von, Schuckmann, K., Pan, Y., Tan, Z., Zhu, Y., Wei, W., Li, G., Ren, Q., Cao, L., and Lu, Y. 2024. New record ocean temperatures and related climate indicators in 2023. Advances in Atmospheric Sciences 41, 1068–1082.

Freund, M.B., Henley, B.J., Karoly, D.J., McGregor, H.V., Abram, N.J., and Dommenget, D. 2019. Higher frequency of central pacific el Niño events in recent decades relative to past centuries. Nature Geoscience 12, 450–455.

Hennemuth, B., Bender, S., Bülow, K., Dreier, N., Keup-Thiel, E., Krüger, O., Mudersbach, C., Radermacher, C., and Schoetter, R. 2013. Statistical methods for the analysis of simulated and observed climate data. CSC Report 13.

Huffman, G., Bolvin, D., Braithwaite, D., Hsu, K., Joyce, R., Kidd, C., Nelkin, E., Sorooshian, S., Tan, J., and Xie, P. 2020. NASA GPM integrated multi-satellite retrievals for GPM (IMERG) algorithm theoretical basis document (ATBD) version 06.1. NASA/GSFC, Greenbelt, MD.

Jiang, J., Liu, Y., Mao, J., Li, J., Zhao, S., and Yu, Y. 2022. Three types of positive Indian Ocean dipoles and their relationships with the south Asian summer monsoon. Journal of Climate 35, 405–424.

Kim, Y.H., Min, S.K., Zhang, X., Sillmann, J. and Sandstad, M., 2020. Evaluation of the CMIP6 multi-model ensemble for climate extreme indices. Weather and Climate Extremes 29, 100269.

Kurniadi, A., Weller, E., Min, S.K, and Seong, M.G. 2021. Independent ENSO and IOD impacts on rainfall extremes over Indonesia. International Journal of Climatology 41, 3640–3656.

Nur'utami, M.N., and Hidayat, R., 2016. Influences of IOD and ENSO to Indonesian rainfall variability: role of atmosphere-ocean interaction in the Indo-pacific sector. Procedia Environmental Science 33, 196–203.

Panggabean, J., Putra, H.F., Habibie, I.M., and Padjajaran, U. 2025. Community-based ecosystem governance model for Indonesia's marine food security 03, 574–586.

Ratna, S.B., Cherchi, A., Osborn, T.J., Joshi, M., and Uppara, U. 2021. The extreme positive Indian Ocean dipole of 2019 and associated Indian summer monsoon rainfall response. Geophysical Research Letters 48, 1–11.

Rentschler, J., Salhab, M., and Jafino, B.A. 2022. Flood exposure and poverty in 188 countries. Nature Communications 13, 1–12.

Sheng, C., Zhang, S., Liu, Y., Wu, G., and He, B. 2023. Interannual impact of tropical southern Atlantic SST on surface air temperature over East Asia during boreal spring. NPJ Climate Atmospheric Science 6, 1–9.

Wati, T., Hadi, T.W., Sopaheluwakan, A., and Hutasoit, L.M. 2022. Statistics of the performance of gridded precipitation datasets in Indonesia. Advances in Meteorology 2022.

Xiao, H.M., Lo, M.H., and Yu, J.Y. 2022. The increased frequency of combined el Niño and positive IOD events since 1965s and its impacts on maritime continent hydroclimates. Scientific Reports 12, 1–11.